International Journal of Pharmaceutics: X 2 (2020) 100042

Contents lists available at ScienceDirect

International Journal of Pharmaceutics: X

journal homepage: www.journals.elsevier.com/international-journal-of-pharmaceutics-x

A novel architecture for achieving high drug loading in amorphous spray dried dispersion tablets

Deanna M. Mudie[a,*], Stephanie Buchanan[a,b], Aaron M. Stewart[a], Adam Smith[a], Kimberly B. Shepard[a], Nishant Biswas[a], Derrick Marshall[a,c], Alyssa Ekdahl[a,d], Amanda Pluntze[a], Christopher D. Craig[a], Michael M. Morgen[a], John M. Baumann[a], David T. Vodak[a]

[a] Global Research and Development, Lonza, Bend, Oregon 97703, USA
[b] Daniel Felix Ritchie School of Engineering & Computer Science, University of Denver, Denver, CO 80210, USA
[c] Pivotal Drug Product Technologies, Amgen, Cambridge, MA 02141, USA
[d] Cockrell School of Engineering, The University of Texas at Austin, Austin, TX 78712, USA

ARTICLE INFO

Keywords:
Amorphous solid dispersion
Spray drying
Concentration sustainment
Bioavailability enhancement
Physical stability
Eudragit L100
Solid dosage form

ABSTRACT

Although Amorphous Solid Dispersions (ASDs) effectively increase bioavailability, tablet mass can be high due to the large fraction of excipients needed to stabilize the amorphous drug in the solid state, extend drug supersaturation in solution and achieve robust manufacturability. The aim of this work was to reduce tablet mass of an ASD tablet comprising a low glass transition temperature (T_g), rapidly crystallizing drug without compromising these key attributes.

In this approach, erlotinib (T_g = 42 °C, T_m/T_g = 1.4 K/K) was spray dried with the high T_g polymer poly (methyl methacrylate-*co*-methacrylic acid) (Eudragit® L100, Evonik) (T_g = 187 °C) to facilitate high drug loading while maintaining physical stability. Hydroxypropyl methylcellulose acetate succinate (HPMCAS) (AQOAT® HF, Shin-Etsu) was granulated with the ASD to extend supersaturation in solution. For comparison, a benchmark ASD was spray dried at a lower drug loading with HPMCAS-H (T_g = 119 °C).

This High Loaded Dosage Form (HLDF) approach reduced tablet mass by 40%, demonstrated similar physical stability and *in vitro* performance as the benchmark and exhibited excellent downstream manufacturability. Strategically combining two different polymers in a tablet to maintain physical stability and sustain supersaturation in solution can decrease tablet mass of some low T_g, rapidly crystallizing amorphous drugs.

1. Introduction

Amorphous Solid Dispersions (ASDs) are widely used bioavailability enhancing formulations for drugs with low solubility and/or slow dissolution rate in gastrointestinal fluids (Van den Mooter, 2012). ASDs comprise an amorphous drug dispersed within a matrix. The amorphous drug provides greater aqueous solubility to aid absorption relative to the crystalline form. The matrix is typically a polymer that acts to stabilize the drug in the amorphous state during storage and in gastrointestinal (GI) fluids (Brouwers et al., 2009; Konno and Taylor, 2006; Taylor and Zhang, 2016).

Drugs with a low glass transition temperature (T_g) and a high ratio of melting point (T_m) to T_g (T_m/T_g (K/K)) tend to recrystallize due to an overall high driving force and low kinetic barrier to crystallization (Friesen et al., 2008). A drug with a high T_m requires high thermal energy to break the crystal lattice, which generally results in a high energy difference between the crystalline and amorphous forms of the drug. This high energy difference can lead to a high thermodynamic driving force for the drug to convert to the lower energy crystalline state. A low T_g indicates a high degree of molecular mobility and therefore a low kinetic barrier to crystallization.

Low T_g, rapidly crystallizing drugs often need a high percentage of dispersion polymer in the ASD to adequately stabilize the drug in the solid state and in solution (Baghel et al., 2016)'(Ting et al., 2015; Ullrich and Schiffter, 2018). For example, a dispersion polymer loading of 75% is common, with dispersion polymer loadings of up to 90–95% being reported. The high percentage of dispersion polymer in the ASD not only results in low drug loading but can also cause poor disintegration. ASDs compressed into tablets may disintegrate slowly when the ASD loading in the tablet exceeds 30–70% (Démuth et al., 2015)' (Agrawal et al., 2016). Poor disintegration is particularly common for neutral polymers, such as polyvinylpyrrolidone (PVP, e.g. K30 grade),

* Corresponding author.
E-mail address: deanna.mudie@lonza.com (D.M. Mudie).

https://doi.org/10.1016/j.ijpx.2020.100042
Received 24 December 2019; Received in revised form 7 February 2020; Accepted 8 February 2020
Available online 19 February 2020

polyvinylpyrrolidone vinyl acetate (PVP VA, i.e. VA 64 grade) and hydroxypropyl methylcellulose (HPMC, e.g. E3 grade) that are soluble across the GI pH range. These polymers hydrate immediately upon introduction into the stomach, resulting in a higher propensity to gel compared to polymers such as Eudragit L100 and HPMCAS that are nearly insoluble at low gastric pH (Goddeeris et al., 2008). Due to the tendency for ASDs to gel, a relatively high fraction of excipients must be added to the tablet formulation to facilitate more rapid disintegration. The addition of certain types of inorganic salts to the formulation has been shown to decrease gelling and improve drug release from ASD tablets (Takano et al., 2019) (Hughey et al., 2013) (Kajiyama et al., 2008). Due to the combined factors of low drug loading in the ASD, and low ASD loading in the tablet, a high tablet mass or multiple tablet units (i.e. high tablet burden) is often required to deliver the prescribed dose.

The acceptable tablet size and number of units depends upon several criteria. For example, dose, indication, age of the targeted population (e.g., adult, pediatric, geriatric), healthy or disease state, desired market image and drug product life cycle all need to be considered. For high dose drugs, tablet burden may be a significant issue. According to Pharmacircle, 24% of all prescription drug products marketed worldwide, including amorphous and non-amorphous drug substances, have doses of 200 mg or greater (PharmaCircle, 2018). Of 22 FDA-approved ASD drug products surveyed according to the maximum dosage strength, more than 50% have maximum dosage strengths greater than 100 mg (Stewart et al., 2020 (in press)). In some cases, accommodating a 100 mg dosage strength for an ASD drug product could require a high tablet mass, which could result in poor patient compliance or be untenable for pediatric and geriatric populations. The tablet mass required to achieve a given dose is determined by the drug loading in the ASD and the ASD loading in the tablet. Typical ASD drug loadings range from 10–40%, whereas ASD loadings in the tablet often range from 40–80%. Assuming these ranges, a total tablet mass of 300–2500 mg would be required to achieve a 100 mg active dose in a single dosage unit. For example, a 25% active ASD with a 50% ASD loading in the tablet would result in a total tablet mass of 800 mg to achieve a 100 mg active dose. The 100 mg dosage strength of the commercial spray dried ASD tablet, Intelence®, has an 800 mg total mass (Voorspoels and Jans, 2008). ASD drug products indicated for infections are likely to require strategies for limiting tablet burden, as 56% of current drug products indicated for infections have doses of 200 mg or greater (PharmaCircle, 2018).

To address high tablet burden, a strategy was developed to maximize the percentage of drug in a rapidly disintegrating ASD dosage form for low T_g, rapidly crystallizing drugs. In this approach, a drug is spray dried with a high T_g polymer to facilitate high drug loading in the ASD (Babcock et al., 2013). To extend drug supersaturation in solution, a concentration sustaining polymer (CSP) is granulated with the ASD prior to tableting (Ozaki et al., 2013) (Xie and Taylor, 2016). In this study, the enteric polymer, poly(methyl methacrylate-*co*-methacrylic acid) (1:1) (Eudragit® L100, Evonik Industries, Essen, Germany) (T_g = 187 °C) Eudragit® L100 was selected as the dispersion polymer due to its high T_g, which is 30–70 °C higher than common dispersion polymers such as HPMCAS, PVP, PVP VA and HPMC (Shepard et al., 2020). Hydroxypropyl methylcellulose acetate succinate (HPMCAS) (T_g = 119 °C) H grade was chosen as the CSP. HPMCAS is a particularly effective CSP due its amphiphilic nature when ionized at small intestinal pH. At pH > ~5, hydrophobic regions of HPMCAS can interact with hydrophobic drugs, and carboxylate groups can interact with the aqueous phase at the drug-water interface to inhibit crystal nucleation and growth (Mosquera-Giraldo et al., 2016) (Price et al., 2019) (Friesen et al., 2008). The H grade of HPMCAS H was chosen for this study since it has the highest percentage of hydrophobic acetyl substitution of the standard HPMCAS grades, allowing it to interact most effectively with hydrophobic drugs. Compared to HPMCAS, Eudragit L100 is typically a less effective CSP. Potential factors contributing to its relative ineffectiveness as a CSP include its hydrophilicity and lack of branches or bulky groups for forming favorable polymer-drug interactions (Mosquera-Giraldo et al., 2016) (Ilevbare et al., 2013).

This work describes use of the HLDF architecture to reduce tablet mass by 40% compared to a typical approach. In a typical ASD formulation the dispersion polymer(s) enables both solid-state physical stability and dissolution rate and/or concentration sustainment in GI fluids. In contrast, the HLDF architecture combines two different polymers, one inside and one outside the ASD to achieve physical stability and concentration sustainment. HLDF and typical 'benchmark' ASDs were assessed for physical stability and tablets were assessed for *in vitro* dissolution performance. Manufacturability of the HLDF tablets was assessed by characterizing tablet attributes after manufacturing at the kilogram scale and assessing flow and mechanical properties of the final blend. Physical stability and *in vitro* performance were found to be comparable for the HLDF and benchmark formulation approaches, and excellent manufacturability was demonstrated for the HLDF architecture.

2. Materials and methods

2.1. Materials

2.1.1. Selection of model drug

Erlotinib is a weak base with poor aqueous solubility and moderate lipophilicity, placing it into the provisional Biopharmaceutics Classification System (BCS) category 2 (Amidon et al., 1995; Dahan et al., 2009; Tóth et al., 2016). Refer to Fig. 1 and Table 1 for the structure and physical properties, respectively. Erlotinib was chosen as a model drug due to its low T_g (42 °C) and tendency to recrystallize both in the solid state and in solution at intestinal pH, as indicated by its high T_m/T_g (1.4 K/K). These attributes made it an ideal candidate for demonstrating the HLDF architecture from a physical property perspective. For example, polymer stabilization is required both in the solid state and in solution to achieve good physical stability and *in vitro* dissolution performance.

To improve low oral bioavailability of the poorly soluble free base, erlotinib is marketed as a hydrochloride salt under the tradename Tarceva®. Common dosages of erlotinib are 100 mg/day (pancreatic cancer) and 150 mg/day (non-small cell lung cancer). It is prescribed fasted due to a positive food effect. In addition, the FDA label recommends avoidance of concomitant use with Proton Pump Inhibitors (PPIs) and modification of the dosing schedule when using H-2 receptor antagonists and antacids due to decreased plasma exposure (Lam et al., 2016) (Ohgami et al., 2018). The 100 mg tablet has a reported absolute bioavailability of 76% (Ranson et al., 2010). The 150 mg Tarceva tablet has an absolute bioavailability of 59% (Frohna et al., 2006). Improving Tarceva, for example, by reducing dosage form size, improving bioavailability or mitigating the food or PPI effect was not a goal of this study.

2.1.2. Material sourcing

Erlotinib free base (> 99% purity) (CAS 183321-74-6) was purchased from LC Laboratories (Woburn, MA, USA) to support drug characterization and lab scale spray drying and from BOC Sciences (Shirley, NY, USA) to support clinical scale spray drying. HPMCAS-H AQOAT® HF was purchased from Shin-Etsu Chemical Co., Ltd. (Tokyo,

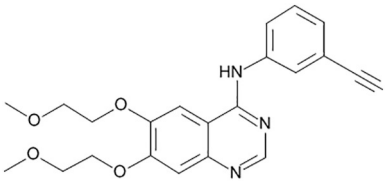

Fig. 1. Erlotinib structure.

Table 1
Erlotinib physicochemical properties.

Property	Value
Molecular mass (g/mol)	393.4
pK_a (basic)	5.3[a]
Log P	2.75[a]
Log D (pH 2)	0.66[a]
T_m (°C)	157[b]
T_g (°C)	42 [b]
T_m/T_g	1.4
Crystalline equilibrium solubility at pH 2 (μg/mL)	1534[c]
Crystalline equilibrium solubility pH 6.5 (μg/mL)	3[d]
Crystalline equilibrium solubility pH 6.5 + 0.5% (*w*/w) FaSSIF powder (μg/mL)	8.6[d]
Crystalline equilibrium solubility pH 6.5 + 1% (*w*/w) FaSSIF powder (μg/mL)	19.7[d]

[a] From reference (Tóth et al., 2016) at 25 °C.
[b] Erlotinib free base Form II. Measured in house.
[c] From reference (Williams et al., 2018).
[d] Measured in house.

Japan). Avicel® PH-101 microcrystalline cellulose was purchased from FMC Corporation (Philadelphia, PA, USA). Foremost® Lactose 310 was purchased from Foremost Farms (Baraboo, WI, USA). Ac-Di-Sol® croscarmellose sodium was purchased from FMC Corporation (Philadelphia, PA, USA). Cab-O-Sil® fumed silica was purchased from Cabot Corporation (Alpharetta, GA, USA). Magnesium stearate was purchased from Macron Fine Chemicals/Avantor (Radnor, PA, USA). Methanol, ethanol, acetonitrile, and acetone were purchased from Honeywell International Inc. (Morris Plains, New Jersey, USA). Hydrochloric acid (HCl), sodium phosphate, potassium phosphate, and sodium chloride were purchased from Sigma Aldrich Chemical Company (St. Louis, Missouri, USA). Fasted state simulated intestinal fluid (FaSSIF) powder purchased from Biorelevant.com Ltd. (London, United Kingdom).

2.2. HLDF formulation development approach

The HLDF architecture is designed to minimize tablet mass for ASDs, while still maintaining good manufacturability, stability and bioperformance. The tablet mass for a given unit dose is determined by the drug loading in the ASD and the ASD loading in the tablet. In this study, the drug loading in the ASD was taken as the highest loading found to be physically stable after storage at 40 °C/75% relative humidity (RH) for 4 weeks as described in Section 3.2. Since a rapidly disintegrating tablet was targeted for this study to facilitate rapid dispersal of ASD particles, the ASD loading in the tablet was taken as the maximum loading resulting in rapid disintegration (i.e. < 3 min) that also provided adequate downstream manufacturability.

The above methodology allowed for tablet size to be minimized for both the HLDF and benchmark formulation architectures. An HLDF tablet with a 350-mg total mass and a drug loading of 29% was manufactured using a 65/35 (% w/w) erlotinib/Eudragit L100 ASD granulated with HPMCAS-H (1:1 HPMCAS-H/erlotinib) as the CSP on kilogram scale processing equipment. A traditional, benchmark ASD tablet with a 575-mg total mass and a drug loading of 18%, comprising a 35/65 erlotinib/HPMCAS-H ASD was used as a positive control. A negative control tablet was also created comprising a 65/35 (% w/w) erlotinib/Eudragit L100 ASD, which was not granulated with HPMCAS. See Table 2 for a summary of tablet compositions. See Table A1 (appendix section A.1) for detailed tablet compositions.

2.3. ASD manufacturing

2.3.1. Lab-scale spray drying

Small scale studies were supported by ASDs made on a lab-scale spray dryer. ASDs were manufactured at drug loadings of 25, 50, 60, 65

Table 2
Tablet formulation compositions.

Tablet formulation [a]	% Drug loading in tablet	Tablet mass (mg)	ASD composition	% ASD in tablet	% External HPMCAS-H in tablet	% Tableting excipients in tablet [b]
HLDF	29	350	65/35 erlotinib/Eudragit L100	44	29	27
Benchmark	18	575	35/65 erlotinib/HPMCAS-H	50	0	50
Negative control	29	350	65/35 erlotinib/Eudragit L100	44	0	56

[a] The majority of excipients (including external HPMCAS-H for the HLDF tablet) are granulated with the ASD. Additional excipients are blended with the granules and the final blend is compressed into tablets. Detailed compositions can be found in Table A.1. in appendix section A.1.
[b] Tableting excipients include Avicel PH 101, lactose monohydrate 310, ac-di-sol, cab-o-sil M5P and magnesium stearate.

and 75% in Eudragit L100, and 25, 35, 50 and 60% in HPMCAS-H. Spray solutions were prepared by dissolving erlotinib and a dispersion polymer (Eudragit L100 or HPMCAS-H) in methanol at the desired ratio of erlotinib to polymer, while maintaining a solids loading of 3% (w/w). A 3% (w/w) solids loading was the maximum loading achievable for the high loaded ASDs based upon the erlotinib solubility in methanol (2.2% (w/w) at room temperature, measured in house using thermogravimetric analysis, data not shown). Solutions were spray dried with an outlet temperature of 45–50 °C and inlet temperature of 150–160 °C on a customized spray dryer (suitable for batch sizes from 0.5–200 g) capable of drying gas flow rates of up to 35 kg/h using a pressure swirl Schlick model 121, size 2.0 spray nozzle (Düsen-Schlick GmbH, Untersiemau, Germany). Spray dried ASDs were placed in a Gruenberg Benchtop Lab Dryer (Thermal Product Solutions, New Columbia, PA) for > 18 h at 35–40 °C to remove residual solvent (RH was not controlled).

2.3.2. Clinical-scale spray drying

Clinical-scale spray drying was performed to generate 65/35 erlotinib/Eudragit L100 ASD for kilogram-scale HLDF tablet manufacturing. Spray solutions were prepared by dissolving erlotinib and Eudragit L100 in methanol at ratio of 65/35 at a solids loading of 3% (w/w). The solids loading was limited by the solubility of erlotinib in methanol (2.2% w/w). Solutions were spray dried with an outlet temperature of 45 °C and inlet temperature of 150–160 °C on a customized clinical-scale spray dryer capable of drying gas flow rates of up to 150 kg/h using a pressure swirl SK-80-16 spray nozzle (Spraying Systems, USA). These spray drying processing parameters were selected to de-risk formation of filament particles that sometimes occurs with Eudragit L100 (Shepard et al., 2020). The batch size was 2.5 kg of ASD. After the spray drying process, spray dried ASDs were placed in an ES2000–12 environmental chamber (Bahnson Environmental Specialties, NC, USA) for > 14 h at 40 °C and 15% RH to remove residual solvent.

2.4. ASD, drug and polymer characterization

2.4.1. Erlotinib crystalline solubility

The crystalline solubility of erlotinib was measured in 1) pH 6.5, 67 mM phosphate, 2) pH 6.5, 67 mM phosphate containing 0.5% (w/w) FaSSIF powder (FaSSIF, Biorelevant Inc), and 3) pH 6.5, 67 mM phosphate containing 1% (w/w) FaSSIF powder. These media were chosen to bracket compositions present in the *in vitro* dissolution tests. See appendix section A.2 for methods.

2.4.2. Powder X-Ray Diffraction (PXRD)

To assess crystallinity of initial and aged samples, XRD patterns were obtained at room temperature using a Rigaku MiniFlex 600 X-Ray diffractometer operating with a copper anode ($K_{\alpha1}$ = 1.5060 Å; $K_{\alpha2}$ = 1.54439 Å) generator set at 45 kV and 15 mA, in 2-theta range 3–40° 2θ, scanned at a rate of 2.5° 2θ per minute in continuous scanning mode, and using a D/teX Ultra high speed detector.

2.4.3. Scanning Electron Microscopy (SEM)

ASDs were assessed for the presence of crystals as well as particle shape and morphology using a Hitachi SU3500 scanning electron microscope (SEM) (Hitachi High Technologies America Inc., Schaumburg, IL). Approximately 0.5 mg of sample was mounted to an aluminum stub with 2-sided carbon tape. The sample was sputter-coated (Hummer Sputtering System, Model 6.2, Anatech Ltd.) with an Au/Pd stage for 10 min at 15 mV, and studied by SEM.

2.4.4. Differential Scanning Calorimetry (DSC)

Melting point, enthalpy of fusion and T_g of the as-received crystalline drug and T_g of the spray dried ASDs were measured using a TA Instruments Q2000 modulated differential scanning calorimeter (TA Instruments-Waters L.L.C, New Castle, DE) equipped with a refrigerated cooling accessory (RCS90). The melting point and enthalpy of fusion of the as-received crystalline drug were measured on heating (10 K/min non-modulated). After heating through the melt, the molten sample was promptly removed from the furnace and quenched into liquid nitrogen (~7200 K/min quench rate) to amorphize the sample. The T_g of the resulting sample was then measured on re-heating (modulated mode at a scan rate of 2.5 °C/min, modulation of ± 1.5 °C/min).

To measure ASD T_g, ASD Samples were prepared as loose powder, loaded into a Tzero pan (TA Instruments) and equilibrated at < 5% RH, 25% RH, 50% RH and/or 75%RH at ambient temperature for up to 18 h. Samples were then crimped with hermetic lids and run in modulated mode at a scan rate of 2.5 °C/min, modulation of ± 1.5 °C/min, and a scan range −40 to 200 °C. A nitrogen gas flow rate of 50 ml/min was used to maintain an inert atmosphere. Unless otherwise stated, reported T_gs are the temperatures at half height of the glass transition. The relationships between T_g and drug loading as well as T_g and relative humidity were assessed and compared between Eudragit L100 and HPMCAS-H dispersion polymers.

2.5. ASD accelerated physical stability studies

HPMCAS-H and Eudragit L100 ASDs (drug loadings of 25, 50, 60, 65 and 75% in Eudragit L100 and 25, 35, 50 and 60% in HPMCAS) were stored at elevated temperature and RH. Approximately 100 mg of each material was placed in a 4-ml glass vial. Each vial was then covered with perforated aluminum foil and transferred to a temperature/humidity-controlled oven (Model ES2000, Environmental Specialties International, lnc., Baton Rouge, LA) at 40 °C/75% RH and allowed to stand undisturbed for 1, 2 and 4 weeks. Samples were then removed from the oven and transferred to a vacuum desiccator for up to 18 h to remove water. After drying, the samples were removed from the vacuum desiccator and stored at 5 °C. Aged ASDs were analyzed for crystallinity using SEM and PXRD and thermal properties using DSC.

2.6. Tablet manufacturing and powder characterization

2.6.1. Small scale manufacturing of benchmark and negative control tablets

The negative control tablet and benchmark tablet were made using a small scale, semi-manual manufacturing process. Briefly, the ASD and intra-granular excipients (See Table A1 in appendix section A.1) were blended and the intra-granular blend was compressed into slugs using a Manesty F3 single station tablet press (Manesty Ltd., Knowsley, England). Slugs were milled using a mortar and pestle and passed through a #20 mesh screen to create the intra-granular blend. The intra-granular blend was blended with extra-granular excipients and lubricated. The final blend was then compressed into tablets at a target Tensile Strength (TS) of 2 MPa using the F3 press. Complete manufacturing details are included in the appendix section A.3.

2.6.2. Kilogram scale manufacturing to make HLDF tablets

HLDF tablets were manufactured at a kilogram manufacturing scale (5-kg pre-granulation blend) to demonstrate the viability of producing tablets comprising a fine particle size excipient (i.e. HPMCAS-HF) external to the ASD. Briefly, the ASD and intra-granular excipients (See Table A1 in appendix section A.1) were blended and lubricated. The intra-granular blend was roller compacted using a Gerteis MINIPACTOR® roller compactor (Gerteis Maschinen + Processengineering AG, Jona, Switzerland). Ribbons were milled through a 1.0 mm square wire mesh screen using the Gerteis in-line mill to create the intra-granular blend. The intra-granular blend was blended with extra-granular excipients and lubricated. The final blend was compressed into tablets using a Korsch XL-100 tablet press (Korsch America, South Easton, MA). Tablets were compressed to a target TS of 2.0 MPa at a 20-rpm turret speed. Additional tablets were produced at different TS values and one additional turret speed (See Table A3 in the appendix

section A.3) to assess the impact of TS and turret speed on disintegration time and friability. Complete manufacturing details are included in the appendix section A.3.

2.7. HLDF powder characterization

Powder and flow properties including bulk density, tapped density, true density and Carr's Index were measured for the intragranular and final blends. Flow function coefficient (ffc) of the final blend was assessed using a Schulze ring shear tester (RST-XS.s, Jenike & Johanson, Tyngsboro, Massachusetts). In addition, Compressibility, Tabletability, Compactability (CTC) profiles of the final blend were generated on an MCC Presster compaction emulator (MCC, East Hanover, NJ) to assess the dependence of strain rate on compression properties. Methods for each measurement can be found in the appendix section A.4.

2.8. Tablet characterization

2.8.1. Disintegration

HLDF, benchmark and negative control tablets were evaluated for disintegration performance in a USP disintegration apparatus (ZT-71 disintegration tester, Erweka, Heusenstamm, Germany) according to the USP method (Convention, 2020). Tablets were placed one each inside of the six tubes within the basket-rack assembly. 750 ml of 0.01 N HCl (pH 2) maintained at 37 ± 2 °C was used as the immersion fluid.

2.8.2. In vitro dissolution performance

The rates and extents of dissolution and precipitation of the HLDF, benchmark and negative control tablets were measured using a custom Controlled Transfer Dissolution (CTD) apparatus. In the CTD apparatus, a drug product is administered in the stomach compartment. Disintegrated drug particles and drug in solution transit from the stomach compartment into the duodenum followed by the jejunum compartment at a user specified fluid emptying rate (See Fig. A1 in appendix section A.4 for a schematic of the apparatus). The CTD apparatus is based upon similar systems in the literature (Bhattachar et al., 2011; Carino et al., 2006; Carino et al., 2010; Takeuchi et al., 2014).

Dissolution testing was performed using two different gastric pH values since variation in gastric pH is known to impact solubility and dissolution of weakly basic drugs and enteric polymers (Mitra and Kesisoglou, 2013) (Monschke and Wagner, 2019). The gastric pH values selected were representative of fasted humans (pH 2.0) and of fasted humans on a PPI (pH 6.0). The duodenal compartment pH was representative of fasted humans (pH 6.5) (Fagerberg and Bergström, 2015; Litou et al., 2016). Fluid compositions and testing parameters are shown in Table 3). At the 100-mg tablet dose, erlotinib was dosed below saturation with respect to crystalline free base solubility at low gastric pH but supersaturated at high gastric pH. Erlotinib was supersaturated with respect to crystalline free base solubility in the duodenum and jejunum compartments for both experiments. For the low gastric pH experiments, concentration vs. time profiles were generated in all compartments using *in situ* UV fiber optic probes (Pion Rainbow™, Pion Inc., Billerica, MA). Second derivative detection at a wavelength range of 376–380 nm (stomach compartment) and 332–336 nm (duodenum/jejunum compartments) was used with a calibration range of 0–216 μg/ml. For the high gastric pH experiments, the detection wavelength range was consistent across all compartments at 332–336 nm using a calibration range of 0–65 μg/ml. Each CTD test was performed in duplicate. Area Under the Curve (AUC) values in the duodenum and jejunum compartments were calculated to compare performance as a function of gastric pH.

2.8.3. Additional tablet characterization

Friability and content uniformity testing were performed on HLDF tablets. See appendix section A.4 for methods.

Table 3
Controlled Transfer Dissolution (CTD) experimental parameters.

Parameter	Value
Dose (mg)	100
Dosing volume (ml)	240
Dosing medium	0.025% (w/w) FaSSIF powder in Milli-Q water
Stomach pH	2.0 or 6.0
Stomach resting volume (ml)	50
Stomach resting and secretion medium	0.01 N HCl + 34 mM NaCl (pH 2), 1e-06 N HCl + 34 mM NaCl (pH 6)
Stomach secretion rate (ml/min)	2
Stomach fluid emptying rate half-life (mono-exponential, min)	15
Duodenum pH	6.5
Duodenum volume (ml)	50
Duodenum resting and secretion medium	1% (w/w) FaSSIF powder[a] in 134 mM phosphate, pH 6.5
Jejunum pH	6.5
Jejunum medium	Gastric + duodenum composition
Jejunum volume	Starts at 0 & increases to 597 ml at 90 min

[a] 1% (w/w) FaSSIF powder is equivalent to 13.4 mM sodium taurocholate. Using these resting and secretion volumes, the range in FaSSIF observed in the duodenal compartment ranges from 1% (w/w) to 0.2% (w/w).

3. Results and discussion

3.1. Drug and ASD characterization

3.1.1. Erlotinib crystalline solubility

The equilibrium crystalline solubilities of erlotinib in pH 6.5 phosphate, pH 6.5 phosphate with 0.5% (w/w) FaSSIF powder, and pH 6.5 phosphate with 1% (w/w) FaSSIF powder at 37 °C can be found in Table 1.

3.1.2. Powder X-Ray Diffraction (PXRD)

PXRD patterns from the ASDs after spray drying were compared to the sharp characteristic diffraction peaks of pure crystalline erlotinib. No diffraction peaks were detected in the ASDs indicating they were amorphous. Diffractograms are presented in Fig. A2 the appendix section A.6.

3.1.3. Scanning Electron Microscopy (SEM)

Morphology of crystalline erlotinib and representative ASDs prior to accelerated stability storage are presented in Fig. A3 in the appendix section A.7. As received, crystalline erlotinib has a plate-like crystal habit. Morphology of the ASDs included collapsed spheres or a mixture of collapsed spheres and fractured collapsed spheres. No crystalline material was observed along the surfaces of the ASDs.

3.1.4. Differential Scanning Calorimetry (DSC)

The T_m of the crystalline erlotinib free base (Form II) measured by DSC was 157 °C, with a heat of fusion of 139 J/g. The T_g of amorphous erlotinib measured by DSC had an onset temperature of 39 °C and a midpoint temperature of 42 °C.

Dry T_g versus drug loading for all ASDs and T_g versus RH for selected ASDs are shown in Fig. 2 and Fig. 3, respectively. All ASDs demonstrated a single T_g suggesting a homogeneous phase of polymer and drug. Dry T_g at a given drug loading is higher for the Eudragit L100 compared to the HPMCAS-H ASDs. For example, the dry T_g of the 60/40 erlotinib/Eudragit L100 ASD is 106 °C, which is 51 °C higher than the HPMCAS ASD with equal active loading (60/40 erlotinib/HPMCAS-H; T_g = 55 °C). The more favorable T_g values of the Eudragit L100 compared to the HPMCAS-H ASDs at a given drug loading is mainly

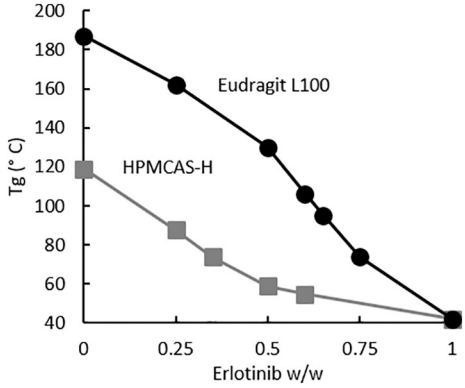

Fig. 2. Glass transition temperature (T_g) versus fraction drug in polymer (w/w) for Eudragit L100 (circles) and HPMCAS-H (squares) Amorphous Solid Dispersions (ASDs).

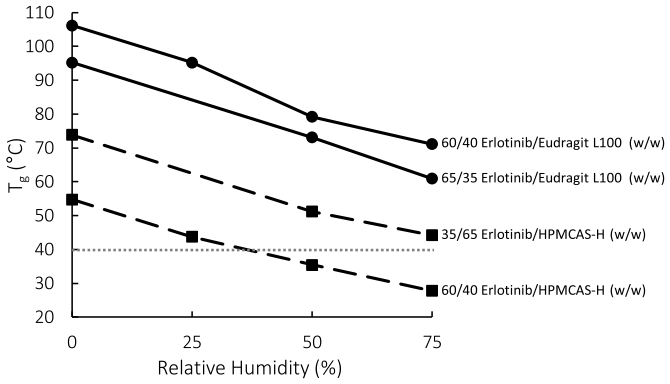

Fig. 3. Glass transition temperature (T_g) versus percent relative humidity (% RH) for selected Eudragit L100 (circles) and HPMCAS-H (squares) Amorphous Solid Dispersions (ASDs). Dashed line represents the storage temperature for the accelerated physical stability studies.

attributed to the higher T_g of Eudragit L100 compared to HPMCAS-H. However, factors such as intermolecular interactions between drug and polymer can also impact dispersion T_g (Khougaz and Clas, 2000; Newman and Zografi, 2019).

The large difference in T_gs between the Eudragit L100 and HPMCAS-H ASDs persists at increasing RH values. For example, at 75% RH the 60/40 erlotinib/Eudragit L100 ASD has a 43 °C higher T_g than the HPMCAS ASD with equivalent drug loading (71 °C vs. 28 °C, respectively). For all ASDs, T_g decreases with increasing RH with approximately the same slope, indicating that the ASDs are plasticized similarly by water. T_g values of selected ASDs and T_g versus RH for additional ASDs are presented in Fig. A4 in the appendix section A.8.

3.2. ASD physical stability

Erlotinib/Eudragit L100 ASDs at drug loadings up to and including 65% (w/w) remained stable throughout the 4-week study. ASD stability was indicated by 1) lack of sharp diffraction peaks in the PXRD, 2) lack of fusing and morphology changes in SEM micrographs 3) a single T_g without melting events in the DSC. At 75% drug loading, fibrous structures were observed in the micrographs after 1 week at 40 °C/75% RH. PXRD indicated characteristic Bragg diffraction peaks that matched a known crystalline form of erlotinib, confirming evidence of recrystallization. The T_g remained equivalent to the initial T_g of the sample and no crystallization was observed via DSC. However, a small endothermic peak was observed at 145 °C.

Benchmark ASDs comprising HPMCAS-H remained stable throughout the 4-week study for drug loadings up to and including 35% (w/w). However, at drug loadings of 50 and 60% (w/w), the benchmark ASDs showed crystallization after 1 week. SEM micrographs showed fusing of the particles and re-crystallization after 1 week for both the 50% and 60% ASDs. These observations were confirmed by evidence of sharp diffraction peaks in the XRD patterns of the 1-week samples. See appendix section A.9 for SEM micrographs, PXRD diffractograms and DSC thermograms of selected ASDs at 0 and 4 weeks.

Table 4
Results of accelerated physical stability testing of Eudragit L100 and HPMCAS-H ASDs.

Dispersion polymer	Drug loading (weight%) in ASD	Results after 4 weeks at 40 °C/75%RH
Eudragit L100	25	Stable (no change)
	50	Stable (no change)
	60	Stable (no change)
	65	Stable (no change)
	75	Unstable (fibrous structures after 1 week)
HPMCAS-H	25	Stable (no change)
	35	Stable (no change)
	50	Unstable – crystals after 1 week
	60	Unstable – crystals after 1 week

Stability data indicated Eudragit L100 provided superior stability at higher drug loadings than the benchmark dispersion polymer HPMCAS-H (See Table 4 for summary of accelerated physical stability testing results.). The more favorable physical stability under stressed conditions of the Eudragit L100 compared to the HPMCAS-H ASDs is likely driven by the higher T_g of Eudragit L100 compared to HPMAS-H. For example, when equilibrated to the 75% RH storage condition, the T_gs of the Eudragit L100 dispersions were all above the 40 °C storage temperature (Fig. 3). The stable 60% (w/w) and 65% (w/w) Eudragit L100 ASDs were 21 °C and 31 °C above the storage temperature, respectively, whereas the non-stable 75% (w/w) Eudragit L100 ASD was only 4 °C above the storage temperature. The stable 25% (w/w) and 35% (w/w) HPMCAS-H ASDs were both 7 °C above the storage temperature, whereas the non-stable 50% (w/w) and 60% (w/w) HPMCAS ASDs were 7 and 12 °C below the storage temperature, respectively. Previous studies have suggested that T_g – T needs to be at least 50 °C for pure amorphous materials (e.g. pure drug) to ensure minimal molecular mobility (Zografi and Newman, 2017) (Hancock et al., 1995). For ASDs formulated with stabilizing polymers, T_g – T values of 5–30 °C are often high enough to impart two-year stability, depending on drug and polymer properties, drug loading and water uptake (Friesen et al., 2008) (Vig and Morgen, 2017) (Yang et al., 2010) (Hancock and Zografi, 1994). The ASDs that remained stable after 4 weeks at 40 °C and 75% RH all had T_g – T values within this range at 75% RH.

3.3. HLDF manufacturability

3.3.1. Clinical scale spray drying

Clinical scale spray drying resulted in desirable ASD morphology characterized by low aspect ratio particles and a lack of filaments as visualized using SEM (Shepard et al., 2020). See Fig. A4 in the appendix section A.7 for the SEM image. Residual methanol present in the ASD after secondary drying was less than 200 ppm as assessed on four replicates using gas chromatography. This value is an order of magnitude below the maximum allowable concentration of 3000 ppm according to International Council for Harmonization (ICH) guidelines.

The spray solution solids loading was maximized to 3% (w/w) based upon the erlotinib solubility in methanol (2.2% (w/w)). At this solids loading spray drying throughput is comparable to what could be achieved for a lower drug loading erlotinib ASD. For example, while a 25/75 erlotinib/Eudragit L100 ASD could achieve an 8% (w/w) spray solution solids loading at a 2% (w/w) erlotinib loading, it would yield the same mass of amorphous erlotinib per unit time as the 65/35

erlotinib/Eudragit L100 ASD sprayed at 3% (w/w) solids loading, assuming comparable spray solution flow rate and yield. In this study, ASD yield assessed prior to secondary drying was high (96%).

3.3.2. Downstream tablet manufacturing

HLDF tablets manufactured on the roller compactor and rotary tablet press met friability, weight uniformity and assay-based content uniformity specifications (See appendix section A.10).

The HLDF formulation is unique compared to a typical spray dried ASD formulation in that a small particle size polymer (HPMCAS-HF) is incorporated into the granulation. Whereas typical intra-granular excipients such as microcrystalline cellulose and lactose have mean particle diameters of at least 50 μm, HPMCAS-HF has a mean particle diameter of 5 μm (Shin-Etsu Chemical Co., 2005). Incorporation of this small particle size excipient during roller compaction was deemed risky due to a potential for poor flowability and excessive fines. Despite this risk, roller compaction of the HLDF intra-granular blend was successful, resulting in good compaction, minimal sticking, minor bypass and low fines. The measured granule size distribution was in line with distributions of conventional ASD granulations manufactured in-house (data not shown).

Roller compaction improved bulk density, tapped density and flowability. Average bulk powder and flow properties are included in Table 5. Flowability measurements were indicative of the successful tableting on the Korsch XL 100 rotary tablet press at 20 and 50 rpm. Avicel PH 102 can serve as a benchmark for assessing whether flowability is adequate for successful tableting on a high-speed tablet press (Sun, 2010). Avicel PH 102 has a Carr's Index of 25.8%, and an ff_c of 6.1 at a 1 kPa pre-consolidation stress and 20% RH (Sun, 2010). Carr's Index of the extra-granular blend in this study (22%) was superior to that of Avicel PH 102. However, the ff_c (4.3) fell below the criterion. While flowability was still acceptable for rotary tableting in this study, flow properties of the extra-granular blend could be further improved through formulation optimization to facilitate manufacturing at higher speeds.

The rotary tablet press and the Presster compaction emulator demonstrated excellent Compressibility, Tabletability and Compactability (CTC) of the extra-granular blend. See Table 6 for Compression Pressure (CP) and Solid Fraction (SF) at each TS produced on the rotary tablet press. CTC profiles generated using the compaction emulator are shown in Fig. 4. See appendix section A.10 for analysis of TS and CP at SF = 0.85. The compaction pressures needed to achieve a TS of 2 MPa on the rotary press and compaction emulator were low and therefore reasonable for manufacturing equipment. A tablet TS of 2 MPa is commonly targeted to achieve strong tablets meeting the USP friability standard (Osei-Yeboah and Sun, 2015; Paul and Sun, 2017). The CP needed to achieve TS = 2 MPa on the compaction emulator at 10 ms (< 60 MPa) was only ~20 MPa higher than what was needed to reach TS = 2 MPa for Avicel PH 102 at 8 ms on the same equipment, as measured by Tye and coworkers (Tye et al., 2005). While an effect of strain rate was observed at higher CP when comparing the 10 ms and 100 ms dwell times, this result was not practically relevant since lower CPs are needed to achieve TS = 2 MPa. The SF needed to achieve TS = 2 MPa (~0.76) measured on the compaction emulator fell between that of Avicel PH 102 (~0.55) and the common tableting excipient, lactose monohydrate (0.80), as measured by Tye and coworkers (Tye et al., 2005).

Table 6
Tableting mechanical properties achieved using Korsch XL 100 (3/8" SRC tooling), 14 MPa pre-compression pressure.

Compression pressure (MPa)	Tensile strength (MPa)	Solid fraction	Turret speed (rpm)/ dwell time (ms)
73	2.0	0.78	20 rpm/81
77	2.0	0.78	50 rpm/32
53	1.2	0.73	20 rpm/81
87	2.8	0.81	20 rpm/81

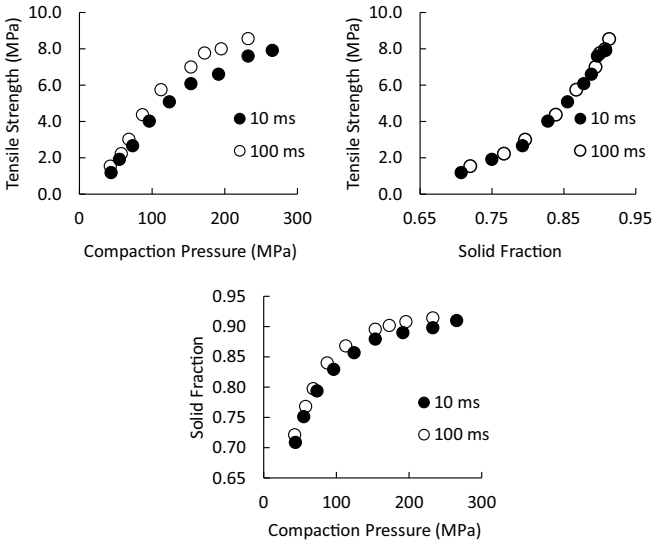

Fig. 4. Compressibility Tabletability Compactability (CTC) profiles generated using the Presster™ compaction emulator at 10 ms (closed circles) and 100 ms (open circles) dwell times.

Table 7
Disintegration testing results.

Tablet type	Tablet tensile strength (MPa)	Turret speed (rpm)	Disintegration time, min average (standard deviation), n = 3
Benchmark	2	N/A (manual press)	0.93 (0.04)
Negative control	2	N/A (manual press)	Did not measure
HLDF	2.0	20	1.1 (0.13)
HLDF	1.2	20	0.5 (0.02)
HLDF	2.8	20	2.4 (0.04)
HLDF	2.0	50	1.1 (0.12)

3.4. Tablet performance

Average disintegration times are listed in Table 7. HLDF tablets produced using the roller compactor and rotary tablet press disintegrated in less than 2.5 min across the TS range of 1.2 – 2.8 MPa, with an average disintegration time of 1.1 min at TS = 2 MPa. Disintegration time increased with an increase in TS. Benchmark tablets disintegrated in less than 1 min. Disintegration testing was not formally performed on each tablet at pH 6 (elevated gastric condition) but demonstrated rapid

Table 5
Average bulk powder and flow properties for intra- and extra-granular novel architecture blends.

Blend	Bulk density (g/cm^3)	Tapped density (g/cm^3)	True density (g/cm^3)	Carr's index (%)	ff_c
Intra-granular	0.22	0.36	1.325	38	N/A
Extra-granular (final blend)	0.44	0.56	1.332	22	4.3

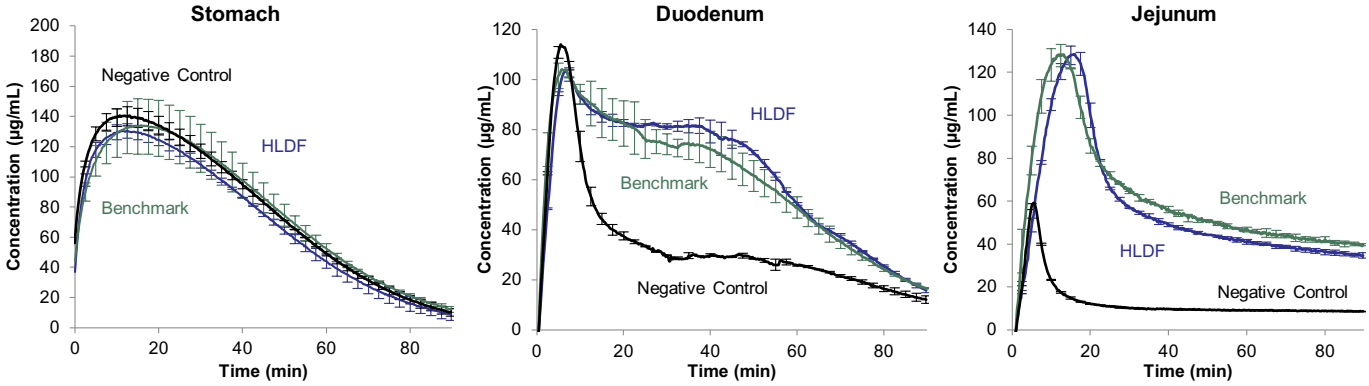

Fig. 5. Concentration time profiles in the stomach, duodenum and jejunum compartments of the Controlled Transfer Dissolution (CTD) test at low (pH 2) gastric pH for High Loaded Dosage Form (HLDF), benchmark and negative control tablets.

(< 2 min) visual disintegration during CTD testing at those conditions.

In vitro dissolution testing demonstrated similar performance between the HLDF tablet and the benchmark tablet at both low (pH 2.0) and high (pH 6.0) gastric pH, whereas the negative control tablet showed inferior performance at high gastric pH due to more rapid crystallization in the duodenum and jejunum. CTD results are shown in Fig. 5 and Fig. 6 for the low gastric pH and high gastric pH tests, respectively. Tabulated data are shown in the appendix section A.10. At low gastric pH, the HLDF and benchmark tablets had duodenal AUC_{0-90} values 1.8 times greater than the negative control tablet. At high gastric pH, the HLDF and benchmark tablets had duodenal AUC_{0-90} values 2.8 times greater than the negative control tablet. At high gastric pH, the HLDF tablet shows less gastric release than the benchmark tablet, which can be attributed to the lower solubility of erlotinib at pH 6 compared to pH 2. Total AUC in the duodenum and jejunum at high gastric pH was 70% of that at low gastric pH for both the HLDF and benchmark, compared to 60% for the negative control.

HLDF tablets showed equivalent *in vitro* performance in the CTD test, while reducing tablet mass by 40% relative to the benchmark tablet. The HLDF tablet significantly outperformed the negative control by delaying precipitation, due to incorporation of HPMCAS-H external to the ASD. External HPMCAS-H was able to provide similar sustainment of supersaturation of erlotinib in both the HLDF and benchmark tablets at both gastric conditions (pH 2.0 and pH 6.0), suggesting that the CSP does not require incorporation into the spray dried ASD intermediate itself, but can be successfully distributed into the final dosage form. Additionally, the HLDF tablet provided similar performance with a lower amount of HPMCAS-H (1:1 erlotinib:HPMCAS-H vs. 1:1.85 erlotinib:HPMCAS-H in benchmark). This information suggests that incorporating the HPMCAS-H outside of the ASD allows for composition optimization without negatively impacting physical stability or manufacturability. This flexibility allows a formulator to optimize the level of CSP for bioperformance.

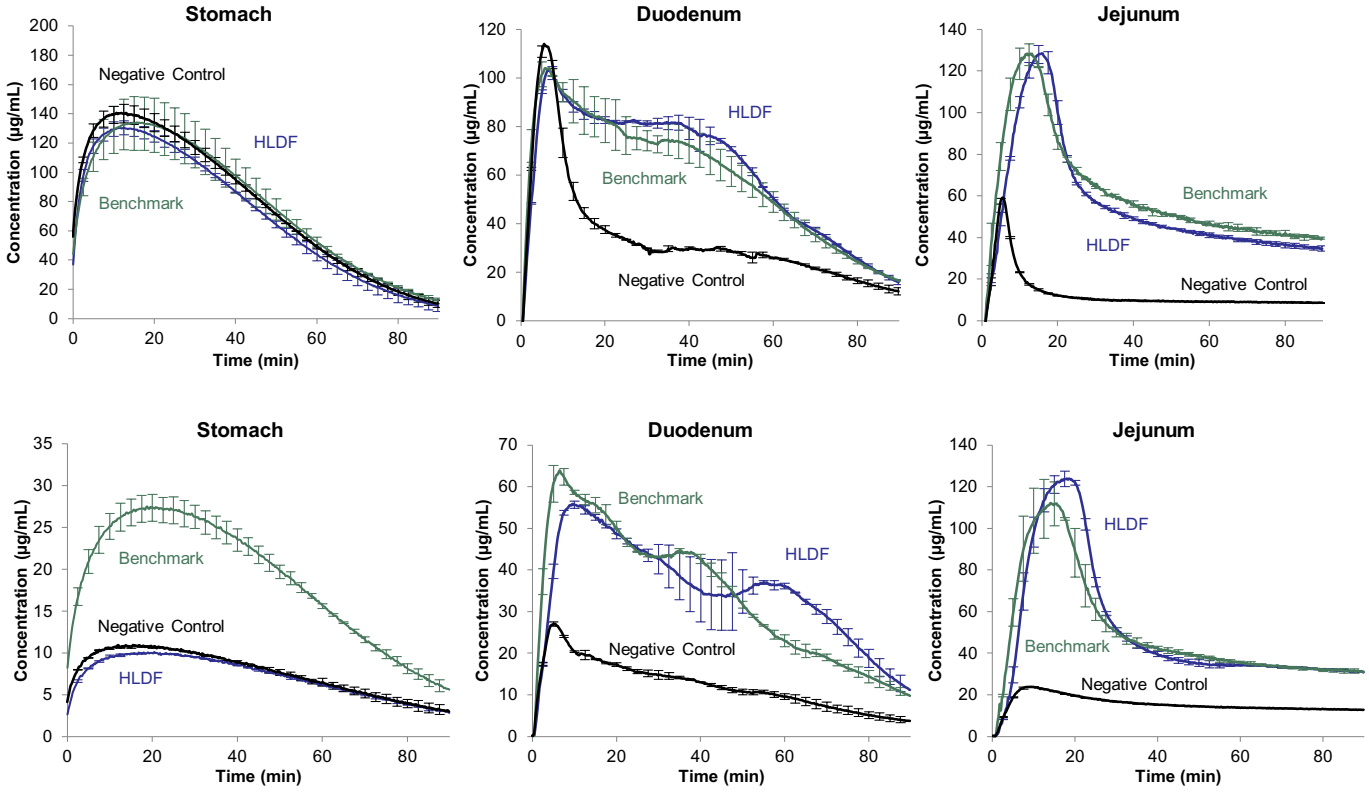

Fig. 6. Concentration time profiles in the stomach, duodenum and jejunum compartments of the Controlled Transfer Dissolution (CTD) test at high (pH 6) gastric pH for High Loaded Dosage Form (HLDF), benchmark and negative control tablets.

Interestingly, differentiation was observed in gastric dissolution rate at elevated gastric pH between the HLDF and benchmark tablets. This result is likely attributed to the "sharper" solubility versus pH profile of Eudragit L100 versus HPMCAS-H, specifically around the pH where both polymers are intended to dissolve. Eudragit L100 has a significantly higher acidic content (ca. 5.6 mM acid/g polymer) compared to HPMCAS-H (0.64 mM acid/g polymer),[1] providing potential benefit in limiting the release of drug at elevated gastric pH (up to ~pH 6), and therefore decreasing the risk of gastric precipitation to a lower energy drug form. Though gastric precipitation was not observed for erlotinib in this study, it is a known risk for poorly water soluble weakly basic drugs that are a focus of the HLDF architecture.

The CTD data presented supports the hypothesis that the HLDF architecture should perform similarly to the lower loaded benchmark tablets and outperform the high loaded negative control tablets. This result would be expected to occur particularly at high doses, where absorption is driven predominately by the ability to maintain high (supersaturated) drug concentrations in the intestine.

4. Conclusions

The current study demonstrates a new high drug loading dosage form architecture for ASDs of rapidly crystallizing poorly soluble drugs. This "HLDF" architecture strategically combines two different polymers, one inside and one outside the ASD, to optimize solubilization performance, physical stability and manufacturability. Using this architecture versus using a single dispersion polymer in the ASD to maintain physical stability and sustain supersaturation can allow equivalent *in vitro* performance while reducing dosage form size. Here we demonstrate the HLDF architecture using the low T_g, rapidly crystallizing drug, erlotinib. For this model drug, using Eudragit L100 as the dispersion polymer and HPMCAS-H as a concentration sustaining polymer (CSP) granulated with the ASD reduced tablet mass by 40% compared to using HPMCAS-H as both the dispersion polymer and the CSP. Physical stability and *in vitro* dissolution performance were comparable for the HLDF architecture and traditional benchmark approach, and excellent manufacturability of the HLDF architecture was demonstrated. This work presents *in vitro* results, demonstrating a promising strategy for decreasing tablet size and/or number of dosage units for drug candidates requiring an amorphous form of the drug to achieve good *in vivo* performance.

Declaration of Competing Interest

The authors declare that they have no known competing financial interests or personal relationships that could have appeared to influence the work reported in this paper.

Acknowledgments

We would like to thank Dr. Changquan Calvin Sun and his laboratory at the University of Minnesota for performing the compaction emulation experiments. We would like to thank Warren Miller for his valuable insights regarding polymer chemistry. The HLDF architecture described herein is the subject of the pending international patent application PCT/IB2019/053836, titled "Solid Dosage Forms with High Active Agent Loading". Applicants/Inventors include Deanna Mudie, Michael Morgen and Kimberly Shepard. The authors declare no additional conflicts of interest. This research did not receive any specific grant from funding agencies in the public, commercial or not-for-profit sectors.

[1] Eudragit L100 acid content calculated from average of 300–330 mg KOH/g dry L100 reported in Evonik technical bulletin. HPMCAS acid content calculated from the succinate assay reported in the certificates of analysis for 17 lots of Shin-Etsu HPMCAS-H.

Appendix A. Supplementary data

Supplementary data to this article can be found online at https://doi.org/10.1016/j.ijpx.2020.100042.

References

Agrawal, A., Dudhedia, M., Deng, W., Shepard, K., Zhong, L., Povilaitis, E., Zimny, E., 2016. Development of tablet formulation of amorphous solid dispersions prepared by hot melt extrusion using quality by design approach. AAPS PharmSciTech 17, 214–232.

Amidon, G.L., Lennernas, H., Shah, V.P., Crison, J.R., 1995. A theoretical basis for a biopharmaceutic drug classification: the correlation of in vitro drug product dissolution and in vivo bioavailability. Pharm. Res. 12, 413–420.

Babcock W, Nightingale J, Shankar R, 2013. Pharmaceutical Solid Dispersions US 8,481, 081 B2, in: Patent, U.S. (Ed.). Bend Research, Inc., USA.

Baghel, S., Cathcart, H., O'Reilly, N.J., 2016. Polymeric amorphous solid dispersions: a review of amorphization, crystallization, stabilization, solid-state characterization, and aqueous solubilization of biopharmaceutical classification system class II drugs. J. Pharm. Sci. 105, 2527–2544.

Bhattachar, S.N., Perkins, E.J., Tan, J.S., Burns, L.J., 2011. Effect of gastric pH on the pharmacokinetics of a BCS class II compound in dogs: utilization of an artificial stomach and duodenum dissolution model and GastroPlus,(TM) simulations to predict absorption. J. Pharm. Sci. 100, 4756–4765.

Brouwers, J., Brewster, M.E., Augustijns, P., 2009. Supersaturating drug delivery systems: the answer to solubility-limited oral bioavailability? J. Pharm. Sci. 98, 2549–2572.

Carino, S.R., Sperry, D.C., Hawley, M., 2006. Relative bioavailability estimation of carbamazepine crystal forms using an artificial stomach-duodenum model. J. Pharm. Sci. 95, 116–125.

Carino, S.R., Sperry, D.C., Hawley, M., 2010. Relative bioavailability of three different solid forms of PNU-141659 as determined with the artificial stomach-duodenum model. J. Pharm. Sci. 99, 3923–3930.

Convention, T.U.S.P., 2020. Disintegration. < 701 > USP43-NF38.

Dahan, A., Miller, J.M., Amidon, G.L., 2009. Prediction of solubility and permeability class membership: provisional BCS classification of the world's top oral drugs. AAPS J. 11, 740–746.

Démuth, B., Nagy, Z.K., Balogh, A., Vigh, T., Marosi, G., Verreck, G., Van Assche, I., Brewster, M.E., 2015. Downstream processing of polymer-based amorphous solid dispersions to generate tablet formulations. Int. J. Pharm. 486, 268–286.

Fagerberg, J.H., Bergström, C.A.S., 2015. Intestinal solubility and absorption of poorly water soluble compounds: predictions, challenges and solutions. Ther. Deliv. 6, 935–939.

Friesen, D.T., Shanker, R., Crew, M., Smithey, D.T., Curatolo, W.J., Nightingale, J.A.S., 2008. Hydroxypropyl methylcellulose acetate succinate-based spray-dried dispersions: an overview. Mol. Pharm. 5, 1003–1019.

Frohna, P., Lu, J., Eppler, S., Hamilton, M., Wolf, J., Rakhit, A., Ling, J., Kenkare-Mitra, S.R., Lum, B.L., 2006. Evaluation of the absolute oral bioavailability and bioequivalence of erlotinib, an inhibitor of the epidermal growth factor receptor tyrosine kinase, in a randomized, crossover study in healthy subjects. J. Clin. Pharmacol. 46, 282–290.

Goddeeris, C., Willems, T., Van den Mooter, G., 2008. Formulation of fast disintegrating tablets of ternary solid dispersions consisting of TPGS 1000 and HPMC 2910 or PVPVA 64 to improve the dissolution of the anti-HIV drug UC 781. Eur. J. Pharm. Sci. 34, 293–302.

Hancock, B.C., Zografi, G., 1994. The relationship between the glass transition temperature and the water content of amorphous pharmaceutical solids. Pharm. Res. 11, 471–477.

Hancock, B.C., Shamblin, S.L., Zografi, G., 1995. Molecular mobility of amorphous pharmaceutical solids below their glass transition temperatures. Pharm. Res. 12, 799–806.

Hughey, J.R., Keen, J.M., Miller, D.A., Kolter, K., Langley, N., McGinity, J.W., 2013. The use of inorganic salts to improve the dissolution characteristics of tablets containing Soluplus(R)-based solid dispersions. Eur. J. Pharm. Sci. 48, 758–766.

Ilevbare, G.A., Liu, H., Edgar, K.J., Taylor, L.S., 2013. Maintaining supersaturation in aqueous drug solutions: impact of different polymers on induction times. Cryst. Growth Des. 13, 740–751.

Kajiyama, A., Takagi, H., Moribe, K., Yamamoto, K., 2008. Improvement of HPMC tablet disintegration by the addition of inorganic salts. Chem. Pharm. Bull. 56, 598–601.

Khougaz, K., Clas, S.D., 2000. Crystallization inhibition in solid dispersions of MK-0591 and poly(vinylpyrrolidone) polymers. J. Pharm. Sci. 89, 1325–1334.

Konno, H., Taylor, L.S., 2006. Influence of different polymers on the crystallization tendency of molecularly dispersed amorphous felodipine. J. Pharm. Sci. 95, 2692–2705.

Lam, L.H., Capparelli, E.V., Kurzrock, R., 2016. Association of concurrent acid-suppression therapy with survival outcomes and adverse event incidence in oncology patients receiving erlotinib. Cancer Chemother. Pharmacol. 78, 427–432.

Litou, C., Vertzoni, M., Goumas, C., Vasdekis, V., Xu, W., Kesisoglou, F., Reppas, C., 2016. Characteristics of the human upper gastrointestinal contents in the fasted state under hypo- and A-chlorhydric gastric conditions under conditions of typical drug – drug interaction studies. Pharm. Res. 33, 1399–1412.

Mitra, A., Kesisoglou, F., 2013. Impaired drug absorption due to high stomach pH: a review of strategies for mitigation of such effect to enable pharmaceutical product development. Mol. Pharm. 10, 3970–3979.

Monschke, M., Wagner, K.G., 2019. Amorphous solid dispersions of weak bases with pH-dependent soluble polymers to overcome limited bioavailability due to gastric pH

variability - an in-vitro approach. Int. J. Pharm. 564, 162–170.
Mosquera-Giraldo, L.I., Borca, C.H., Meng, X., Edgar, K.J., Slipchenko, L.V., Taylor, L.S., 2016. Mechanistic design of chemically diverse polymers with applications in oral drug delivery. Biomacromolecules 17, 3659–3671.
Newman, A., Zografi, G., 2019. Commentary: considerations in the measurement of glass transition temperatures of pharmaceutical amorphous solids. AAPS PharmSciTech 21, 26.
Ohgami, M., Kaburagi, T., Kurosawa, A., Doki, K., Shiozawa, T., Hizawa, N., Homma, M., 2018. Effects of proton pump inhibitor coadministration on the plasma concentration of erlotinib in patients with non-small cell lung cancer. Ther. Drug Monit. 40, 699–704.
Osei-Yeboah, F., Sun, C.C., 2015. Validation and applications of an expedited tablet friability method. Int. J. Pharm. 484, 146–155.
Ozaki, S., Kushida, I., Yamashita, T., Hasebe, T., Shirai, O., Kano, K., 2013. Inhibition of crystal nucleation and growth by water-soluble polymers and its impact on the supersaturation profiles of amorphous drugs. J. Pharm. Sci. 102, 2273–2281.
Paul, S., Sun, C.C., 2017. Dependence of friability on tablet mechanical properties and a predictive approach for binary mixtures. Pharm. Res. 34, 2901–2909.
PharmaCircle, L., 2018. www.pharmacircle.com.
Price, D.J., Ditzinger, F., Koehl, N.J., Jankovic, S., Tsakiridou, G., Nair, A., Holm, R., Kuentz, M., Dressman, J.B., Saal, C., 2019. Approaches to increase mechanistic understanding and aid in the selection of precipitation inhibitors for supersaturating formulations – a PEARRL review. J. Pharm. Pharmacol. 71, 483–509.
Ranson, M., Shaw, H., Wolf, J., Hamilton, M., McCarthy, S., Dean, E., Reid, A., Judson, I., 2010. A phase I dose-escalation and bioavailability study of oral and intravenous formulations of erlotinib (Tarceva, OSI-774) in patients with advanced solid tumors of epithelial origin. Cancer Chemother. Pharmacol. 66, 53–58.
Shepard, K.B., Adam, M.S., Morgen, M.M., Mudie, D.M., Regan, D.T., Baumann, J.M., Vodak, D.T., 2020. Impact of process parameters on particle morphology and filament formation in spray dried Eudragit L100 polymer. Powder Technol. 362, 221–230.
Shin-Etsu Chemical Co., L, 2005. NF Hypromellose Acetate Succinate Shin-Etsu AQOAT Enteric Coating Agent. Tokyo, Japan.
Stewart, A., Mudie, D., Yates, I., Hall, R., 2020. Development & biopharmaceutical characterization of amorphous solid dispersions. In: Patel, D. (Ed.), Supersaturated Drug Delivery Systems (SDDSs): Development and Biopharmaceutical Characterization. Springer International Publishing AG, Switzerland (in press).
Sun, C.C., 2010. Setting the bar for powder flow properties in successful high speed tableting. Powder Technol. 201, 106–108.
Takano, R., Maurer, R., Jacob, L., Stowasser, F., Stillhart, C., Page, S., 2019. Formulating amorphous solid dispersions: impact of inorganic salts on drug release from tablets containing Itraconazole-HPMC extrudate. Mol. Pharm.
Takeuchi, S., Tsume, Y., Amidon, G.E., Amidon, G.L., 2014. Evaluation of a three compartment in Vitro gastrointestinal simulator dissolution apparatus to predict in Vivo dissolution. J. Pharm. Sci. 103, 3416–3422.
Taylor, L.S., Zhang, G.G.Z., 2016. Physical chemistry of supersaturated solutions and implications for oral absorption. Adv. Drug Deliv. Rev. 101, 122–142.
Ting, J.M., Navale, T.S., Jones, S.D., Bates, F.S., Reineke, T.M., 2015. Deconstructing HPMCAS: excipient design to tailor polymer-drug interactions for oral drug delivery. ACS Biomater. Sci. Eng. 1, 978–990.
Tóth, G., Jánoska, Á., Szabó, Z.-I., Völgyi, G., Orgován, G., Szente, L., Noszál, B., 2016. Physicochemical characterisation and cyclodextrin complexation of erlotinib. Supramol. Chem. 28, 656–664.
Tye, C.K., Sun, C., Amidon, G.E., 2005. Evaluation of the effects of tableting speed on the relationships between compaction pressure, tablet tensile strength, and tablet solid fraction. J. Pharm. Sci. 94, 465–472.
Ullrich, A., Schiffter, H.A., 2018. The influence of polymer excipients on the dissolution and recrystallization behavior of ketoconazole: application, variation and practical aspects of a pH shift method. Eur. J. Pharm. Biopharm. 133, 20–30.
Van den Mooter, G., 2012. The use of amorphous solid dispersions: a formulation strategy to overcome poor solubility and dissolution rate. Drug Discov. Today Technol. 9, e79–e85.
Vig, B., Morgen, M., 2017. Chapter 30 - formulation, process development, and scale-up: spray-drying amorphous solid dispersions for insoluble drugs. In: Qiu, Y., Chen, Y., Zhang, G.G.Z., Yu, L., Mantri, R.V. (Eds.), Developing Solid Oral Dosage Forms, Second edition. Academic Press, Boston, pp. 793–820.
Voorspoels, J.F.M., Jans, E.M.J., 2008. Combination formulations comprising darunavir and etravirine. In: Organization, W.I.P.
Xie, T., Taylor, L.S., 2016. Improved release of celecoxib from high drug loading amorphous solid dispersions formulated with polyacrylic acid and cellulose derivatives. Mol. Pharm. 13, 873–884.
Yang, J., Grey, K., Doney, J., 2010. An improved kinetics approach to describe the physical stability of amorphous solid dispersions. Int. J. Pharm. 384, 24–31.
Zografi, G., Newman, A., 2017. Interrelationships between structure and the properties of amorphous solids of pharmaceutical interest. J. Pharm. Sci. 106, 5–27.